



**Nonmonotonic heat flux trends of a boundary-heated granular gas**Andrew Hong  and Aaron Morris \**Mechanical Engineering Department, Purdue University, West Lafayette, Indiana 47907, USA*

(Received 28 February 2022; accepted 13 June 2022; published 29 June 2022)

By means of the direct simulation Monte Carlo method, the effect of rarefaction on the heat fluxes and the hydrodynamics of a granular gas bounded by thermal walls is investigated. The heat flux is found to evolve nonmonotonically with the particle inelasticity due to the competition between the particle inelasticity and rarefaction. The former enhances the heat flux, and the latter reduces the heat flux. As the particles become more inelastic, the onset of the heat flux diminishment due to rarefaction is found to be signaled by a temperature gradient collapse. The same temperature gradient convergence, which precedes the rarefied-reduced heat flux, is also found as the applied temperature gradient is increased.

DOI: [10.1103/PhysRevE.105.064903](https://doi.org/10.1103/PhysRevE.105.064903)**I. INTRODUCTION**

The hallmark characteristic of granular systems is the inelastic particle-particle collisions. Granular systems serve as excellent models for several industrial processes and natural phenomena [1,2]. Under external forcing, granular particles can behave as a fluid. The fluid-like behavior of granular systems motivated several groups to develop a granular hydrodynamic theory [3–7]. The granular hydrodynamic equations, which resemble the familiar Navier-Stokes (NS) equations, are found from the inelastic Boltzmann equation by considering the first-order solutions following a Chapman-Enskog expansion [8]. The granular NS order solutions have served as the foundational equations to explain various granular fluid phenomena.

In recent years, there has been growing interest in understanding the *nonhydrodynamic* behavior of rarefied granular gases. By nonhydrodynamic, we refer to the fluid phenomena which are not captured by the NS description. From simulations, there is a growing body of literature which has identified nonhydrodynamic phenomena in both granular and molecular gases, such as the Knudsen-minimum paradox [9,10], shear-induced heat fluxes [11,12], and temperature bimodality [9,12]. It has been shown from analytical solutions that a large number of these anomalous fluid phenomena can be described by considering the Burnett order terms [13,14].

However, the analytical solutions are often limited to quasielastic particles. It is unclear whether the existing theory is applicable to particles which are highly inelastic. Furthermore, the bulk of granular gas simulations often consider gases under shear; there is a noticeable scarcity in studies which consider a bounded rarefied granular gas which is not sheared. We believe this is because it would seem that additional heat fluxes from the Burnett order solutions are shear induced. From the generalized Fourier conduction law proposed by Pan *et al.*, the additional heat flux contributions

in a stationary rarefied molecular gas come from the third spatial derivative of the temperature; these high-order effects go beyond the Burnett order. While Risso and Cordero developed analytical solutions for rarefied granular gases using a 14-moment method [15], their solutions are applicable only to quasielastic particles.

To elucidate the rarefaction, or higher order, effects on a granular gas, we consider the case of a low inelasticity granular gas bounded by isothermal walls. This case was previously considered by Brey and Cubero, where they sought to formulate a Newtonian description for quasielastic particles bounded by equal-temperature walls [16]. Reyes *et al.* later extended the work by accounting for non-Newtonian effects [7], allowing their analytical solutions to be valid beyond the quasielastic limit. However, in each of the previous works, the solutions are of NS and Burnett order, respectively.

Analytical solutions for equations beyond the Burnett order are extremely difficult to determine. Therefore, we instead use numerical means by employing the direct simulation Monte Carlo (DSMC) method, a method popular for studying rarefied gases [17]. This paper begins by first briefly describing the DSMC method in Sec. II. The DSMC results are compared to the analytical solutions given by Reyes *et al.* [7], which are outlined in Sec. III. The case of equal temperature walls is first considered. In Sec. IV, the temperatures and temperature gradients from DSMC and theory are first compared. The heat fluxes are then divulged in Sec. V. We then determine if there exists relatively simple modifications to the solutions given by Reyes *et al.* which account for rarefaction effects. We then consider unequal temperature walls in Sec. VI.

**II. THE DIRECT SIMULATION MONTE CARLO (DSMC) METHOD**

Unlike other molecular dynamic methods, the DSMC method utilizes stochastic collisions, making it a popular and computationally efficient tool for simulating rarefied gases. The general procedure for the DSMC method is widely available, and detailed descriptions may be found here [17,18]. We

\*morri353@purdue.edu

will only show the necessary changes to extend the original DSMC method given by Bird [17] to solve for granular gases and how the boundaries are handled.

Inelastic particles lose a proportion of their relative velocity after colliding with one another. The pre- ( $\mathbf{v}$ ) and postcollisional ( $\mathbf{v}'$ ) velocities between particles  $i$  and  $j$  are related through the following,

$$\mathbf{v}_{i,j}' = \mathbf{v}_{i,j} \pm \frac{1+\alpha}{2} (\mathbf{v}_r \cdot \hat{\mathbf{k}}) \hat{\mathbf{k}}, \quad (1)$$

where  $\hat{\mathbf{k}}$  is the unit vector between the centers of the particles at contact, or the apse line,  $\alpha$  is the restitution coefficient, and  $\mathbf{v}_r = \mathbf{v}_i - \mathbf{v}_j$  is the relative velocity. For the scope of this paper, the boundaries are modeled as diffuse walls with a defined wall temperature,  $T_w$ . Particles that come into contact with the thermal boundaries have their tangential,  $v_t$ , and normal,  $v_n$ , velocities randomly sampled from the Gaussian and Maxwell-inflow [19] distributions, respectively,

$$v_t = \sqrt{\frac{k_B T_w}{m}} \mathcal{N}(0, 1) \quad (2)$$

$$v_n = \sqrt{-\log(\mathcal{R})} \sqrt{\frac{2k_B T_w}{m}} \mathcal{N}(0, 1), \quad (3)$$

where  $\mathcal{N}(0, 1)$  is a normally distributed random number with mean zero and variance one, and  $\mathcal{R}$  is a uniformly distributed random number.

To model the bounded granular gas, we define two isothermal walls along the  $x$  direction. The mean of the two wall temperatures is kept constant as one. The remaining boundaries are periodic. The lengths of the system in the  $x$ ,  $y$ , and  $z$  directions are  $[L, W, H] = [20, 10, 10]\lambda$ . The mean free path is defined as  $\lambda = 1/(\sqrt{2}\bar{n}\pi d^2)$ , where  $\bar{n}$  is the number density, the overline indicates a mean value, and  $d$  is the particle diameter. The system is discretized into 80 collision cells along the  $x$  direction. The initial particle velocities are sampled from the Maxwell-Boltzmann distribution with an initial temperature of  $T = 1$ . All particles are identical with diameters ( $d$ ) and masses ( $m$ ) chosen as one. The mean number density is chosen as  $\bar{n} = 0.05$ . The restitution coefficient is assumed to be constant and not vary with the relative velocity. The particles are assumed to interact via a hard-sphere potential, and the particle cross section is then  $\sigma_c = \pi d^2$ .

Unlike continuum models, the hydrodynamic characteristics may be directly sampled from the particle positions and velocities. The cell-averaged density ( $\rho$ ), temperature ( $T$ ), and heat flux ( $\mathbf{q}$ ) are found as

$$\rho = \frac{1}{N_t} \sum_{N_t} \frac{1}{V_{\text{cell}}} \left( \sum_{i \in \text{cell}} m_i \right), \quad (4)$$

$$T = \frac{1}{N_t} \sum_{N_t} \frac{1}{3N} \left[ \sum_{i \in \text{cell}} m_i (c_i \cdot c_i) \right], \quad (5)$$

$$\mathbf{q} = \frac{1}{N_t} \sum_{N_t} \frac{1}{V_{\text{cell}}} \left[ \sum_{i \in \text{cell}} m_i \mathbf{c}_i (c_i \cdot \mathbf{c}_i) \right], \quad (6)$$

where the right summation is over all particles in the collision cell, and the left summation is over  $N_t$  time steps.  $V_{\text{cell}}$  is the volume of the cell,  $\mathbf{c}_i = \mathbf{v}_i - \mathbf{u}$  is the peculiar velocity

of particle  $i$ ,  $\mathbf{v}_i$  is the particle velocity, and  $\mathbf{u}$  is the bulk velocity of the cell the particle resides in. Since the system and its gradients are trivial in the  $y$  and  $z$  directions, only the macroscopic variations in the  $x$  direction ( $q_x$ ) are considered.

### III. ANALYTICAL SOLUTIONS FOR ISOTHERMAL WALLS

The density, momentum, and energy balance equations are given as

$$D_t n + n \nabla \cdot \mathbf{u} = 0, \quad (7)$$

$$D_t \mathbf{u} + (mn)^{-1} \nabla \mathbf{P} = 0, \quad (8)$$

$$D_t T + \frac{2}{3n} (\mathbf{P} : \nabla \mathbf{u} + \nabla \cdot \mathbf{q}) = -T \zeta, \quad (9)$$

where  $D_t = \partial/\partial t + \mathbf{u} \cdot \nabla$  is the material derivative,  $n$  is the number density,  $\mathbf{u}$  is the bulk velocity,  $m$  is the particle mass,  $\mathbf{P}$  is the stress tensor,  $T$  is the temperature, and  $\mathbf{q}$  is the heat flux. There is an additional cooling term,  $\zeta$ , that arises due to the inelastic particle-particle collisions. In the case of zero applied shear, the bulk velocity vanishes ( $\mathbf{u} = 0$ ) and the solutions given by Refs. [7,16] are nearly identical, only differing slightly in their evaluation of the thermal conductivity. At steady state, Eq. (7) equates an identity, and Eqs. (8) and (9) reduce to

$$\nabla \mathbf{P} = 0, \quad (10)$$

$$\nabla \cdot \mathbf{q} = -\frac{3}{2} n T \zeta. \quad (11)$$

Equation (10) indicates that the pressure is uniform.

The heat flux requires that the cooling rate,  $\zeta$ , be known up to the second order. It can be shown that the first-order cooling rate vanishes for the case of no shear [3]. In the dilute and quasielastic limit, the cooling rates from the second-derivative spatial gradients were found to be several orders of magnitude smaller than the thermal conductivity [3]. Consequently, we estimate the cooling rate only by its zeroth-order contribution.

The constitutive equation for the heat flux takes the form

$$\mathbf{q} = -\kappa \nabla T - \mu \frac{T}{n} \nabla n. \quad (12)$$

The second term on the right-hand side is a Dufour-like contribution which has no direct analog in molecular gases. Given the pressure is constant, by substituting in the hydrostatic pressure,  $p = nT$ , Eq. (12) can be rewritten as

$$\mathbf{q} = -\psi \nabla T, \quad \psi = \kappa - \mu. \quad (13)$$

The cooling rate and transport coefficients are expressed in terms of the NS transport coefficients,

$$\zeta_0 = \zeta_0^* \frac{p}{\eta_0}, \quad (14a)$$

$$\psi = \psi^* \kappa_0, \quad (14b)$$

$$\psi^* = (\kappa^* - \mu^*), \quad (14c)$$

where the NS shear viscosity ( $\eta_0$ ) and thermal conductivity ( $\kappa_0$ ) are defined as

$$\kappa_0 = \frac{15\eta_0}{4m}, \quad \eta_0 = \frac{5}{16d^2} \sqrt{\frac{mT}{\pi}}. \quad (15)$$

The reduced values, indicated by asterisks, vary only with  $\alpha$ . Here, we use the analytical expressions for the reduced thermal conductivity and cooling rate given by Brey *et al.* for a low-density granular gas [3],

$$\zeta_0^* = \frac{5}{12}(1 - \alpha^2) \left(1 + \frac{3}{16}a_2\right), \quad (16)$$

$$\kappa^* = \frac{2}{3} \frac{1 + 2a_2}{v_k^* - 2\zeta_0^*}, \quad (17)$$

and

$$\mu^* = 2\zeta_0^* \left( \kappa^* + \frac{2a_2}{3\zeta_0^*} \right) (2v_\mu^* - 3\zeta_0^*)^{-1}, \quad (18)$$

where

$$v_k^* = v_\mu^* = \frac{1 + \alpha}{3} \left[ 1 + \frac{33}{16}(1 - \alpha) + \frac{19 - 3\alpha}{512}a_2 \right] \quad (19)$$

and

$$a_2 = \frac{16(1 - \alpha)(1 - 2\alpha^2)}{81 - 17\alpha + 30(1 - \alpha)\alpha^2}. \quad (20)$$

Combining Eqs. (13)–(18) yields

$$\frac{d}{dx} \left( \kappa_0 \frac{dT}{dx} \right) = -\frac{3}{2} \frac{\zeta}{\psi^*} p, \quad (21)$$

where we now only consider the  $x$  component. To solve Eq. (21), the differential equation can be linearized by considering the following change of variables,  $ds = \nu(x)dx$ , where  $\nu(x)$  is the local collision frequency. Detailed derivations may be found in Refs. [6,7,16]. Here we only quote the final result for the case of zero shear (Eq. (5.40) in Ref. [7]),

$$|x - x_0| = l_0 \left| \sqrt{\frac{T}{T_0} \left( \frac{T}{T_0} - 1 \right)} + \sinh \sqrt{\frac{T}{T_0} - 1} \right|, \quad (22)$$

where  $x_0$  is where the system reaches its minimum temperature,  $T = T_0$ , and

$$l_0 \equiv \frac{wT_0^{1/2}}{2K}, \quad w^2 \equiv \frac{|\Phi|}{2m^2\gamma^2}, \quad (23)$$

where

$$K = \frac{pd^4}{\sqrt{m}\Lambda}, \quad \Lambda = \frac{5}{16\sqrt{\pi}}. \quad (24)$$

In the notation we have used, the term  $\gamma$  evaluated at zero shear is

$$\gamma = \frac{1}{5} \frac{\zeta^*}{\psi^*} \quad (25)$$

and

$$\Phi \equiv -2mB\gamma - \frac{1}{2}A^2. \quad (26)$$

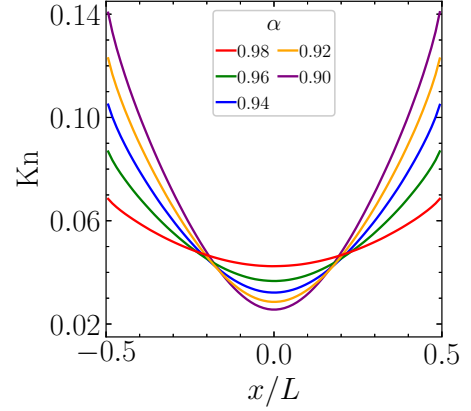


FIG. 1. The local Knudsen values are shown from DSMC for varying  $\alpha$ .

The coefficients,  $A$  and  $B$ , are related to the constraints at an arbitrary location within the domain.

In the case of equal temperature walls, the hydrodynamics are symmetric about the middle of the domain, where we will define  $x = 0$  to be. Note that this would imply  $x_0 = 0$ . The system is coolest at the centerline and has the following constraints,

$$\frac{dT}{dx}(x = 0) = 0, \quad T(x = 0) = T_0, \quad (27)$$

which lead to  $A = 0$  and  $B = T_0$ .

#### IV. CONVERGENT TEMPERATURES AND TEMPERATURE GRADIENTS

We first consider the case of equal-temperature walls where the wall temperatures,  $T_w$ , are set to one. This system is particularly convenient in studying the combined effects of  $\alpha$  and rarefaction. As the particles are made more inelastic, the particles tend to cluster more densely around the center of the domain. Subsequently, the boundaries and regions surrounding the boundaries become more rarefied as shown by the local Kn numbers in Fig. 1. The local Knudsen number is defined as  $\text{Kn} = \lambda/L$ , where the mean free path is evaluated using the local number density. At the boundaries, it is clear the local Kn increases with decreasing  $\alpha$ . At the center of the system, the reverse is true where the local Kn value decreases with decreasing  $\alpha$ . In other words, with stronger particle inelasticity, the boundaries become more rarefied and the interior becomes more dense.

In deriving Eq. (22), the effect of the granular Knudsen layer is neglected. However, the granular Knudsen layer was previously found to be relatively thick [20], and neglecting the boundary layer effects may lead to qualitatively different behavior in the bulk. It is helpful then to determine the extent the granular Knudsen layer effects change the general hydrodynamics in comparison to what is found in DSMC. Plotting the theoretical temperatures requires some care since the quantity,  $l_0$ , requires that the pressure and minimum temperature must be known. A proper comparison between DSMC and theory should limit the amount of information provided by DSMC to theory. Therefore, either the DSMC pressure or the minimum

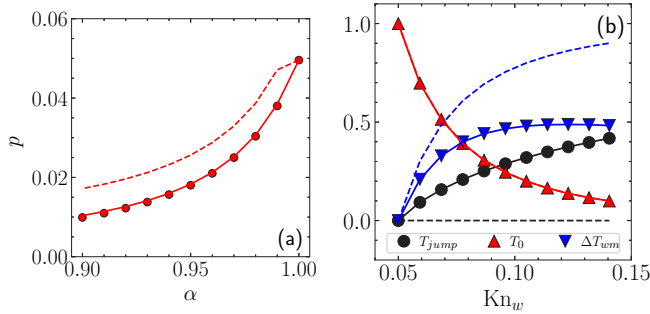


FIG. 2. (a) The pressures are plotted for each  $\alpha$ . Equation (22) is plotted as lines where the solid and dashed lines are with and without the temperature jump,  $T_{\text{jump}}$  modification, respectively. (b)  $T_{\text{jump}}$  (black),  $T_0$  (red), and  $\Delta T_{\text{um}} = T(L) - T_0$  (blue) are plotted against the Knudsen values at the wall. Because the system is symmetric, only the right half of the domain is shown. Markers in both plots indicate DSMC results.

temperature,  $T_0$ , should be provided. The remaining unknown for either case would be found by matching the temperature of the solution at the boundary with the wall temperature. Here, we choose to provide  $T_0$  from DSMC and determine the correct pressures to satisfy the boundary condition. In the left panel of Fig. 2, the pressures are shown. As denoted by the dashed line, we see that the pressures are generally larger than what is found in DSMC. This is expected because the temperature jump at the boundary is ignored. From the right panel of Fig. 2, the temperature jump, defined as  $T_{\text{jump}} = T_w - T(L)$ , is plotted as a function of the Knudsen value at the wall,  $\text{Kn}_w$ . As previously mentioned,  $\text{Kn}_w$  is inversely proportional to  $\alpha$ . It is clear that the temperature jump is significant and cannot be ignored. More interesting is how similar the temperature jump grows with respect to  $T_0$  with increasing rarefaction. To compare the two, the gas temperature at the wall is compared to the minimum temperature and is defined as  $\Delta T_{\text{um}} = T(L) - T_0$ . From the theoretical solutions, the values of  $\Delta T_{\text{um}}$  tend to grow where the growth rate reduces with lower  $\alpha$ . On the other hand, the growth rate of  $\Delta T_{\text{um}}$  reduces more rapidly, exhibiting a plateau after around  $\text{Kn}_w = 0.10$ . While the qualitative characteristics are mostly found from the theory, there are clear quantitative differences. Recovering quantitative agreement in the pressure and  $\Delta T_{\text{um}}$  is surprisingly simple. What we find is that if we modify the boundary conditions for Eq. (22) such that the temperature jump found in DSMC is accounted for, the correct pressures and  $\Delta T_{\text{um}}$  are recovered. These are indicated by the solid lines in Fig. 2.

A similar modification is often used in molecular gases where the boundary condition takes the form

$$T_w - T(L) = C_J \left. \frac{dT}{dx} \right|_w, \quad (28)$$

where  $C_J$  is some constant and  $(dT/dx)_w$  is the temperature gradient at the wall. It is important to note that this modified boundary condition is difficult to use as the temperature gradient tends to diverge near the boundary [20,21]. Normally, the temperature gradient is extrapolated from the temperature profile found within the interior of the gas. However, as seen

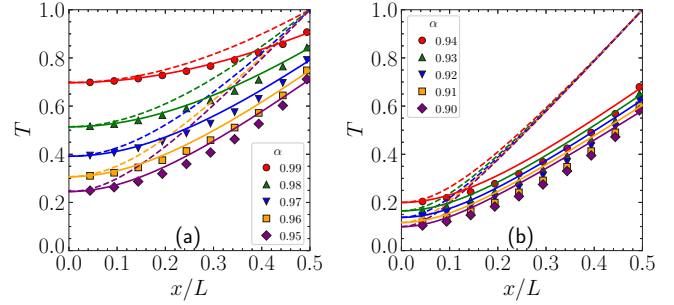


FIG. 3. The temperatures are plotted against the normalized lengths for restitution coefficients ( $\alpha$ ) ranging from (a) 0.99 to 0.95 and (b) 0.94 to 0.90. The solid and dashed lines are the theoretical temperature profiles given by Eq. (22) with and without the temperature jump modification, respectively. Because the system is symmetric, only the right half of the domain is shown. The markers are the measured DSMC temperatures.

from the temperature plots in Fig. 3, such an extrapolation is ambiguous since even at the quasielastic limit ( $\alpha = 0.99$ ) the temperature profiles in the interior of the domain are noticeably different whether the temperature jump is accounted for or not.

But if the temperature jump were known *a priori*, the theoretical temperatures do show good agreement with the DSMC temperatures. There remains minor disagreement as the  $\alpha$  goes beyond the quasielastic limit. For  $\alpha < 0.95$ , Eq. (22) with the modified boundary condition tends to overestimate the temperatures. Without the modified boundary condition, the analytical solutions deviate considerably with the DSMC solutions at all  $\alpha$  considered.

While a modification to the boundary condition seems sufficient in extending the previous theory to rarefied granular gases, this is untrue, as seen from the temperature gradient plots in Fig. 4. At the boundaries, the theory predicts a temperature gradient which appears to asymptote whereas the DSMC temperature gradients diverge. The DSMC results are in agreement with what was previously found from molecular dynamic simulations [20]. In the interior, the DSMC temperature gradients are also lower than what is predicted from theory, an observation first made by Brey *et al.* [16]. The theory shows a qualitative disagreement with DSMC throughout the domain.

What is particularly unusual is that the DSMC temperature gradients converge as  $\alpha$  decreases. The same convergence is absent from theory, whether the temperature jump is ac-

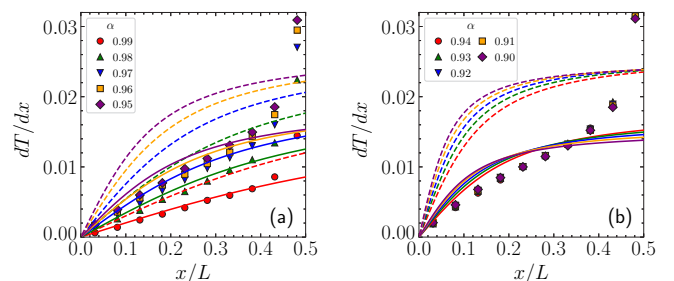


FIG. 4. Same as Fig. 3 but for the temperature gradients.

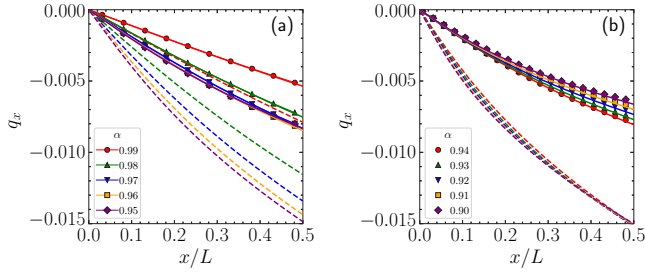
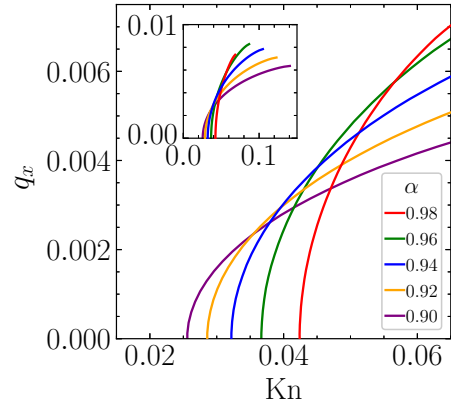


FIG. 5. Same as in Fig. 3 but for the heat fluxes.

counted for or not. We do note that the analytical temperature gradients without the boundary condition modification do converge adjacent to the boundary. The collapse of the temperature gradients is in agreement with the asymptotic  $\Delta T_{um}$  seen in Fig. 2. It is important to note that the temperature gradient convergence is uniform, occurring near the boundaries where the gas becomes increasingly rarefied and in the interior where the gas becomes more dense. Given the dynamics of the system, the gradual convergence of the temperature gradients is likely correlated with the increasing rarefaction of the gas near the boundaries. This temperature gradient convergence is significant because if we take Eq. (28) to be true, then, because the wall temperature is constant, the temperature jump only varies with the constant  $C_J$ . The constant  $C_J$  should vary with the properties of the gas or  $\alpha$ . From numerical fitting, we find that  $T_{\text{jump}} \propto \epsilon^{0.61}$  where  $\epsilon = (1 - \alpha^2)/6$  is often called the inelasticity parameter. To our knowledge, such a temperature gradient convergence in granular gases had not been previously reported.

## V. HEAT FLUX TRENDS

One of the consequences of the temperature gradient collapse is that the heat flux decreases with lower  $\alpha$  beyond the quasielastic limit. From Eq. (13), the heat flux scales with the temperature, the reduced thermal conductivity,  $\psi^*$ , and the temperature gradient. By definition,  $\psi^*$  decreases with  $\alpha$ . The temperature must decrease as the particles become more inelastic. This then leaves the temperature gradient as a primary indication of how the heat flux evolves with  $\alpha$ . For lower  $\alpha$ , the DSMC temperature gradients remains constant, and thus the heat flux must reduce with smaller  $\alpha$ . Near the quasielastic limit, we might expect that the heat flux would increase due to the growing temperature gradient as seen from Fig. 4. In short, the heat flux should first increase then decrease as the particles become more inelastic. To verify this, the theoretical and DSMC heat fluxes are shown in Fig. 5. With more inelastic particles, if the temperature jump is neglected, the theory predicts a heat flux which at first monotonically increases but then rapidly converges in  $\alpha$ . The DSMC heat fluxes show a similar initial evolution where the heat fluxes converge as  $\alpha$  decrease. However, further decreasing  $\alpha$ , the DSMC heat fluxes show an inverted evolution where the heat flux magnitudes decrease. Similar to what we found for the temperature profiles, if the temperature jumps are accounted for, the heat flux evolution from theory is in excellent agreement with DSMC. However, the agreement between DSMC and theory with the temperature jump accounted for is un-

FIG. 6. The local DSMC heat fluxes are plotted for varying  $\alpha$  against the local Knudsen value. The main plot is truncated to improve clarity where the full range of data is shown in the inset.

expected given the qualitative difference in the temperature gradients as seen in Fig. 4. That is, despite a misrepresentation of the temperature gradient, the theoretical heat fluxes agrees with DSMC. This contradiction is confounding. We suspect that the Fourier law of heat conduction is not appropriate for rarefied gases. A more generalized conduction law is likely needed, similar to the one proposed by Pan *et al.* for molecular gases [22]. Further investigation of this discrepancy is out of the scope of this study. Returning to the heat flux evolution, we suspect the nonmonotonic evolution of the heat flux is tied to the increased rarefaction at the boundaries. It is then useful to see how the heat flux evolves with the local Kn values, which are plotted in Fig. 6. We note that the critical  $\alpha$ , below which the heat flux begins to decrease, is highly dependent on the local Kn. For examples, at  $\text{Kn} = 0.06$ , the heat flux monotonically decreases with  $\alpha$ . For  $\text{Kn} = 0.045$ , the heat flux only decreases if  $\alpha \leq 0.96$ .

The Kn dependence on the heat flux evolution can be physically understood as a competition between the rarefaction and particle inelasticity. Rarefaction tends to reduce the heat flux since the interparticle collisions are relatively few; collisions are necessary to form temperature gradients. The inelasticity has the opposite effect where the increased dissipation should tend to accentuate the temperature gradient between the gas and the walls by reducing the mean temperature of the gas. That is, the heat flux is enhanced by the particle inelasticity and attenuated by the rarefaction. To some extent, these observations have been noted previously. However, here we have shown that the qualitative expectations of the rarefaction and inelastic effects are intimately correlated with the evolution of the hydrodynamic gradients, i.e., the temperature gradient. To be more specific, the onset of significant rarefaction effects is signified by the convergence in the temperature gradients as the particle inelasticity is strengthened.

## VI. UNEQUAL TEMPERATURE WALLS

The nonmonotonic heat flux evolution seen for the case of equal temperature walls appears to be a direct consequence of the increased rarefaction of the system. This then begs the question if the nonmonotonic heat flux trend may also be

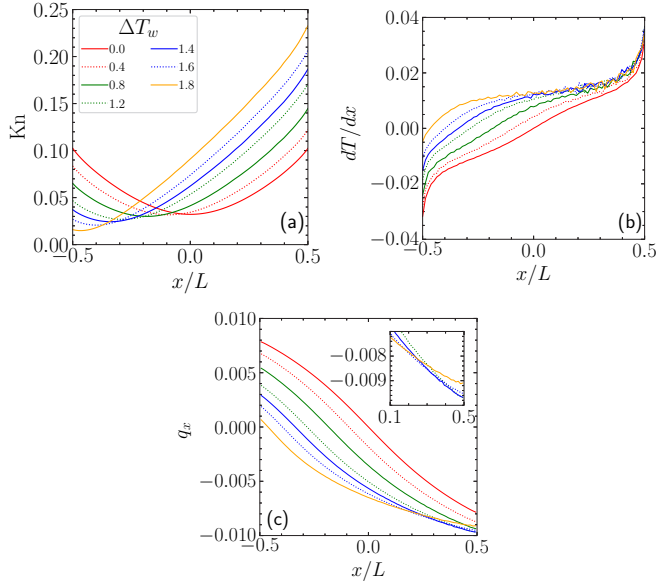


FIG. 7. The (a) local Knudsen value, (b) temperature gradient, and (c) heat flux for  $\alpha = 0.94$  from DSMC are plotted for different wall temperature differences,  $\Delta T_w$ . The inset in the heat flux plot shows the heat fluxes for  $\Delta T_w$  ranging from 1.4 to 1.8 near the right boundary.

found under a different rarefying mechanism. To determine this, we simulate a granular gas bounded by unequal temperature walls. The restitution coefficient is fixed, and the applied temperature gradient is gradually increased. The dimensions of the system are kept the same as before. The mean of the two wall temperatures is kept fixed as one. The left and right wall temperatures are in the ranges 0.2–1 and 1–1.8, respectively. We refer to each set of wall temperatures by their wall temperature difference,  $\Delta T_w = [0, 1.6]$ . The restitution coefficients range from 0.9 to 1.0 as before. Unlike the case where the wall temperatures are equal, and  $\alpha$  is varied, only the hot, right boundary becomes more rarefied while the cold, left boundary becomes more dense, as seen from the Knudsen plot in Fig. 7. Similar to before, the rarefied region near the hot boundary shows the same rarefaction signature: The temperature gradients appear to converge. Once again, the convergent temperature gradients appear to correlate with the nonmonotonic heat flux evolution, except now with respect to  $\Delta T_w$ . From the inset of the heat flux plot in Fig. 7(c), the crossover in the local heat flux near the hot boundary, which indicates a heat flux decrease, is highlighted. We also briefly note that at the cold boundary, the evolution of the hydrodynamics and heat fluxes are qualitatively different. The temperature gradients do not converge, and the heat flux evolves monotonically as the applied temperature gradient increases. This is expected since the gas near the cold boundary becomes increasingly dense, and the rarefaction effects become increasingly negligible. The plots in Fig. 7 are for the case of  $\alpha = 0.94$ . In Fig. 8, the heat fluxes at the hot wall,  $q_{x,H}$ , for several other  $\alpha$  are shown. Note that the heat fluxes shown in Fig. 8 are negative. We first note that the nonmonotonic heat flux evolution with respect to  $\alpha$  can be found for a chosen  $\Delta T_w$ . Additionally,

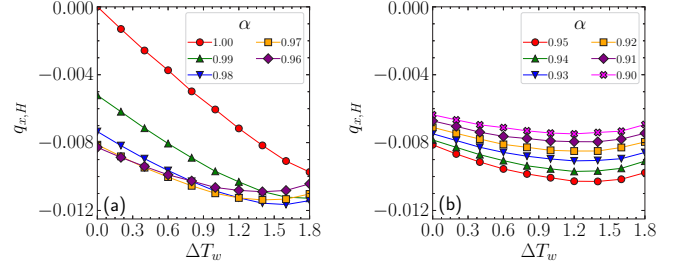


FIG. 8. The heat flux at the hot boundary ( $q_{x,H}$ ) is plotted for different wall temperature differences,  $\Delta T_w$ . The restitution coefficients,  $\alpha$ , range from (a) 1.00 to 0.96 and (b) from 0.95 to 0.90. Lines are drawn as guides.

we find that for a chosen  $\alpha$ , there is, in general, a maximum heat flux magnitude with respect to  $\Delta T_w$ . This suggests that the heat flux near the hot boundary does not always increase as we apply a stronger temperature gradient. For quasielastic particles ( $\alpha = 0.99$ ), the dip, which represent the maximum heat flux magnitude, is not visible. Earlier we found that the onset of the heat flux decrease requires a sufficiently low  $\alpha$  for a given Kn (Fig. 6). We believe the heat flux maxima exists for the quasielastic case but lies outside the range of temperature gradients we investigated here.

## VII. CONCLUSION

In summary, we investigate the rarefaction effects on the evolution of the hydrodynamics and heat fluxes of a bounded granular gas. We find that the heat flux exhibits a non-monotonic heat flux evolution as the particles become more inelastic or the applied temperature gradient is strengthened. The nonmonotonic evolution of the heat flux can be physically understood as a competition between the particle inelasticity and the rarefaction. The former tends to increase the heat flux by steepening the temperature gradient; the latter tends to decrease the heat flux by collapsing the temperature gradients. The onset of significant rarefaction effects, which causes a heat flux decrease, carries a distinct hydrodynamic signature: the convergence of the temperature gradients. The temperature gradient collapse is significant as it implies the temperature jump only depends on a constant if the boundary condition given by Eq. (28) is assumed to be true.

The previous theory given by Reyes *et al.* can be shown to have good quantitative agreement with the DSMC results if the boundary conditions are modified with the temperature jumps found in DSMC. However, while the heat fluxes between the modified theory and DSMC show excellent agreement, the temperature gradients are in qualitative disagreement. This is unusual since the heat flux as given by Eq. (12) is proportional to the temperature gradient. We believe the contradiction is a shortcoming of the Fourier law of heat conduction. Further investigation is needed to correct the constitutive relation for the heat flux to bring consistency between the divergent temperature gradient and nondivergent heat fluxes found from DSMC.

## ACKNOWLEDGMENTS

Acknowledgment is made to the Donors of the American Chemical Society Petroleum Research Fund (PRF 60475-DNI9) for support (or partial support) of this research. We would also like to acknowl-

edge the Halstead Computing Cluster at Purdue University for providing the necessary resources for the work presented here. We would also like to thank the anonymous reviewers for bringing to our attention Refs. [7,16], which provided clear analytical solutions to compare to.

- 
- [1] W. D. Fullmer and C. M. Hrenya, The clustering instability in rapid granular and gas-solid flows, *Annu. Rev. Fluid Mech.* **49**, 485 (2017).
  - [2] I. Goldhirsch, Rapid granular flows, *Annu. Rev. Fluid Mech.* **35**, 267 (2003).
  - [3] J. J. Brey, J. W. Dufty, C. S. Kim, and A. Santos, Hydrodynamics for granular flow at low density, *Phys. Rev. E* **58**, 4638 (1998).
  - [4] E. L. Grossman, T. Zhou, and E. Ben-Naim, Towards granular hydrodynamics in two dimensions, *Phys. Rev. E* **55**, 4200 (1997).
  - [5] V. Garzó and J. W. Dufty, Hydrodynamics for a granular binary mixture at low density, *Phys. Fluids* **14**, 1476 (2002).
  - [6] F. V. Reyes and J. S. Urbach, Steady base states for Navier-Stokes granular hydrodynamics with boundary heating and shear, *J. Fluid Mech.* **636**, 279 (2009).
  - [7] F. V. Reyes, A. Santos, and V. Garzó, Steady base states for non-Newtonian granular hydrodynamics, *J. Fluid Mech.* **719**, 431 (2013).
  - [8] S. Chapman and T. G. Cowling, *The Mathematical Theory of Non-uniform Gases: An Account of the Kinetic Theory of Viscosity, Thermal Conduction, and Diffusion in Gases* (Cambridge University Press, Cambridge, UK, 1990).
  - [9] R. Gupta and M. Alam, Hydrodynamics, wall-slip, and normal-stress differences in rarefied granular poiseuille flow, *Phys. Rev. E* **95**, 022903 (2017).
  - [10] C. Cercignani and A. Daneri, Flow of a rarefied gas between two parallel plates, *J. Appl. Phys.* **34**, 3509 (1963).
  - [11] M. Alam, R. Gupta, and S. Ravichandir, Shear-induced heat transport and the relevance of generalized Fourier's law in granular poiseuille flow, *Phys. Rev. Fluids* **6**, 114303 (2021).
  - [12] F. J. Uribe and A. L. Garcia, Burnett description for plane Poiseuille flow, *Phys. Rev. E* **60**, 4063 (1999).
  - [13] N. Sela and I. Goldhirsch, Hydrodynamic equations for rapid flows of smooth inelastic spheres, to Burnett order, *J. Fluid Mech.* **361**, 41 (1998).
  - [14] S. Saha and M. Alam, Non-Newtonian stress, collisional dissipation, and heat flux in the shear flow of inelastic disks: A reduction via Grads moment method, *J. Fluid Mech.* **757**, 251 (2014).
  - [15] D. Risso and P. Cordero, Dynamics of rarefied granular gases, *Phys. Rev. E* **65**, 021304 (2002).
  - [16] J. J. Brey and D. Cubero, Steady state of a fluidized granular medium between two walls at the same temperature, *Phys. Rev. E* **57**, 2019 (1998).
  - [17] G. A. Bird, *Molecular Gas Dynamics and the Direct Simulation of Gas Flows* (Clarendon Press, London, 1994).
  - [18] T. Pöschel and T. Schwager, *Computational Granular Dynamics: Models and Algorithms* (Springer Science & Business Media, Berlin, 2005).
  - [19] A. L. Garcia and W. Wagner, Generation of the Maxwellian inflow distribution, *J. Comput. Phys.* **217**, 693 (2006).
  - [20] J. E. Galvin, C. M. Hrenya, and R. D. Wildman, On the role of the Knudsen layer in rapid granular flows, *J. Fluid Mech.* **585**, 73 (2007).
  - [21] C. M. Hrenya, J. E. Galvin, and R. D. Wildman, Evidence of higher-order effects in thermally driven rapid granular flows, *J. Fluid Mech.* **598**, 429 (2008).
  - [22] L. S. Pan, D. Xu, J. Lou, and Q. Yao, A generalized heat conduction model in rarefied gas, *EPL* **73**, 846 (2006).